Journal of Nuclear Science and Technology

ISSN: 0022-3131 (Print) 1881-1248 (Online) Journal homepage: https://www.tandfonline.com/loi/tnst20

Characterization of aerosols from RDD surrogate compounds produced by fast thermal transients

Fidelma Giulia Di Lemma, Jean-Yves Colle, Markus Ernstberger & Rudy J.M. Konings

To cite this article: Fidelma Giulia Di Lemma, Jean-Yves Colle, Markus Ernstberger & Rudy J.M. Konings (2016) Characterization of aerosols from RDD surrogate compounds produced by fast thermal transients, Journal of Nuclear Science and Technology, 53:3, 391-401, DOI: 10.1080/00223131.2015.1050473

To link to this article: https://doi.org/10.1080/00223131.2015.1050473

Journal of Nuclear Science and Technology, 2016
Vol. 53, No. 3, 391–401, http://dx.doi.org/10.1080/00223131.2015.1050473

Taylor & Francis
Taylor & Francis Group

ARTICLE

Characterization of aerosols from RDD surrogate compounds produced by fast thermal transients

Fidelma Giulia Di Lemma[a,b*], Jean-Yves Colle[a], Markus Ernstberger[a] and Rudy J.M. Konings[a,b†]

[a]*European Commission, Joint Research Centre, Institute for Transuranium Elements, P.O. Box 2340, 76125 Karlsruhe, Germany;*
[b]*Department of Radiation Science and Technology, Faculty of Applied Sciences, Delft University of Technology, Delft, 2629 JB, The Netherlands*

(*Received 27 November 2014; accepted final version for publication 8 May 2015*)

Experimental tests have been performed to characterize the aerosols representative of radiological dispersion devices (RDDs, a.k.a. "dirty bombs") by applying to chosen surrogate compound rapid high temperature transients, vaporizing the sample and forming aerosols mainly by rapid cooling of the vapour. The materials, which were tested in their non-radioactive form, had been chosen from the radioactive sources widely used in industries and nuclear medicine applications, Co, CsCl, Ir and $SrTiO_3$. Our analyses permitted the characterization of the inhalable fraction of the aerosols released, and the study of the influence of cladding materials on the aerosol release and on its characteristics.

Keywords: particle size; experimental data; radioactivity; source term; radiological dispersion devices; aerosol characterization

1. Introduction

Over the past few years, "dirty bombs" detonations have been of particular interest for international nuclear security analyses, in view of the attention focused on terrorist attacks after 9/11. "Dirty bombs" are bombs created by coupling a conventional explosive with a highly radioactive material with the aim of releasing radioactivity in the environment. Terrorist organizations are believed to be interested in such weapons to spread panic among the population and inflict economic damage. It should be emphasized, as reported by many authors (e.g. [1,2]), that although the purpose behind the use of radiological dispersion devices (RDDs) is not to destroy a city or cause a high number of fatalities, they can have the major long-term effect of increasing cancer cases mainly related to the inhalation of radioactive particles[2,3]. To calculate the impact of RDDs on the population, the quantification of the release (total mass and activity) and its description (size distribution, chemical composition and isotopic composition) is necessary (a.k.a. the source term analysis). As reported by Andersson et al. [4], a better description of the source term is needed, as dispersion calculations are highly sensitive to the input parameters.

In a previous paper [5], we have demonstrated the feasibility of laser heating to produce aerosols from a range of different materials. The present study aims at studying the interactions occurring in the vapour phase influencing aerosol formation in the inhalable fraction. This is performed by vaporizing surrogate inactive materials to simulate radioactive sources that could be misused in RDDs, and by analysing the influence of other components of the radioactive source on the aerosol characteristics. In this particular study, we have focused on evaluating the influence of the cladding materials on the aerosol release. These are materials used as containment and shield for the radioactive source, and have a high probability of reacting with the source. Following a detonation, the cladding materials and the radioactive source are partially dispersed in bigger fragments and blown away, while a part "could interact when in the vicinity of the fireball, as it could be entrained into the turbulent eddies within the fireball" [6]. Once in the fireball the material is vaporized, it can interact chemically in the gaseous phase. Our tests consisted of separate effect studies, performed for a number of sources (Co, CsCl, Ir and $SrTiO_3$) using different cladding materials (tungsten and/or stainless steel). Finally, attention has

*Corresponding author. Email: fidelma.dilemma@gmail.com
†Present address: European Commission, Joint Research Centre, Institute for Transuranium Elements, P.O. Box 2340, 76125 Karlsruhe, Germany.

been focused on evaluating the chemical and elemental composition as a function of particles size (measured by aerodynamic equivalent diameter, or AED). The AED of particles is an important parameter influencing the aerosol transport behaviour in the environment and the risk associated with the inhalation of the particles.

The influence of other source components and environmental materials on the aerosol release from RDDs has been reported by several authors [6–8]. Lee and coworkers [8] studied the interaction of the explosive and soil with a simulated CsCl source and observed the formation of mixed aerosols containing both carbonaceous materials and the simulated source material, and a different ratio of Cs and Cl in the aerosols. However, they could not assess the cause of such effects. Harper et al. [6] tested simulated full-size devices for a wide range of source materials, and concluded that other surrounding materials (such as soil) can interact with the radioactive materials by agglomeration and/or coagulation and affect the size of the "radioactive" particles. Such a complete simulation of an RDD in an integral test is not the goal of our experiments. The aim of our study is instead a deeper understanding of the aerosol formation process, identification of the chemical interactions taking place with other materials and their influence on the aerosol characteristics, which can be performed under simplified controlled laboratory conditions.

2. Experimental

2.1. Instrumentation and experimental procedure

The set-up applied in our study has been described in detail in [5]. In this paper, we just summarize its main features for clarification. Fast laser heating is used to vaporize samples and to form aerosols. With this technique, extreme heating transients can be achieved, e.g. reaching temperatures higher than 3000 K, with heating rates higher than 30000 K/s. The vapour so formed then condenses rapidly in the colder air environment (at room temperature), forming aerosols. These are collected by different systems and on different substrates, depending on the post-analyses to be performed. By using a MOUDI impactor for the collection of the aerosols, it is possible to divide the particles by their AED. This enables us to perform characterization of the particles as a function of their size, and also to obtain their size distribution by weighing the substrates before and after the experiments. SEM/EDX (Vega Tescan model TS5130LSH or a FEI Philips XL 40) was applied for the analysis of the elemental composition, morphology and geometrical size. Raman spectroscopy (Jobin Yvon T64000 spectrometer) was used for the identification of the aerosol phases. Such instruments and their application in our studies have been described in our previous work [5]. The sample holder, used in these tests, consisted of a vertical tube in which the sample was posed on the same horizontal support, and the geometry and the distance between the source and collecting substrates were kept constant. This modification, with respect to the sample holder presented in [5], was performed to avoid aerosol losses in the bends.

Our analyses have shown that a complete simulation of the detonation process is not possible with this set-up, due to the difficulty in controlling and scaling the shock wave in our experiments (e.g. detonation shock waves have an impact pressure up to 450 GPa [9,10]). However, this system is useful to simulate the process of rapidly expanding hot gases involved in the detonation (up to approximately 5500 K in the microsecond range [9,10]) and to study the gaseous interactions. Following an explosion, high temperatures can be reached, which will volatilize part of the source and of the cladding materials. These hot gases will be ejected in a cooler environment. In this scenario, supersaturation conditions will be achieved and homogeneous nucleation of aerosols from the gas will be the dominant process and the contribution of heterogeneous nucleation will be minimal. On the other hand, debris or fragments may act as sinks for the aerosols by agglomeration and producing micrometre-size particles which will rapidly settle. The particles produced with our set-up in the nanometric size range have been compared to the results of integral tests by Lee et al. [8] and have showed similar features. This suggests that our experimental set-up is able to produce representative aerosols in the nanometric size range, which are formed by homogeneous nucleation from the vapour phase released during dirty bomb detonations.

Fast laser heating reproduced a bimodal aerosol size distribution, as observed also in integral tests[6–8]. Although the fractional release between these two size ranges cannot reproduce the scenario of a real detonation, the study and comparison of these aerosols can help in understanding the phenomena taking place, and the difference between solid and vaporized phases. The first peak of the size distribution (in the nanometric size range) is generated, as explained also in [5], by the condensation of the high temperature vapour released, followed by their agglomeration. The second peak (in the micrometre size range) has been related to mechanical shock, similarly to what observed in the precedent integral experiments [6–8]. In the integral tests, the micrometre-size aerosols were generated by explosive blasts, while in our tests this was related to a stochastic effect generated by the thermal shock on the unmelted brittle pellet or on the produced liquid layer, due to rapid laser heating. Thus, it is not possible to reproduce a real mechanical blast and the pressure encountered in an RDD detonation by the use of laser heating. As a result, the quantities of these micrometre-size particles are not representative of the quantities of particles ejected by the detonation blast, but by analysing and comparing them to the nanometric particles formed by the vaporization process, important information can be obtained.

Table 1. Radionuclides of concern for RDD production (as reported in [11]).

Radionuclide	Typical physiochemical form	Application	Activity
^{60}Co	Metal	Sterilization irradiator	Up to 400 000 TBq
		Nuclear medicine	Up to 1000 TBq
^{90}Sr	Ceramic ($SrTiO_3$)	Thermoelectric generator	1000–10 000 TBq
^{137}Cs	Salt (CsCl)	Sterilization irradiator	Up to 400 000 TBq
		Nuclear medicine	Up to 1000 TBq
^{192}Ir	Metal	Industrial radiography	Up to 5 TBq
^{226}Ra	Salt ($RaSO_4$)	Nuclear medicine	Up to 5 TBq
^{238}Pu	Ceramic (PuO_2)	Thermoelectric generator	Up to 5 TBq
^{241}Am	Pressed ceramic powder (AmO_2)	Well logging source	Up to 1 TBq
^{252}Cf	Ceramic (Cf_2O_3)	Well logging source	Up to 0.1 TBq

2.2. *Samples*

The materials tested were chosen from the most commonly used radioactive sources and tested in their natural isotopic composition. A list of the sources most commonly feared to be acquired by terrorists to create an RDD is shown in **Table 1**. From these, the highest activity and the most available sources were tested. The source materials chosen were Co, CsCl, Ir and $SrTiO_3$. The samples were pellets of 5 mm diameter, obtained by pressing commercial powders (from Alfa Aesar) by a hydraulic press. For Co also, solid discs were tested [5], but no difference was observed for the aerosol characteristics.

Different laser pulses were tested to rapidly heat part of the sample surface. However, for the same conditions applied (square laser pulse 3000 W, lasting 60 ms), the temperature reached on the surface of the tested materials was different. This is due to the different thermodynamic and surface properties of the materials used (shown in Table 3). Temperature was measured by a rapid high temperature pyrometer [5]. Finally, the amount of material vaporized varied between the different materials tested, ranging from a few mg to tens of mg.

Powder mixtures, containing the cladding materials (tungsten and/or stainless steel) and the simulated source materials to be tested, have been pressed to create the samples for studying the influence of cladding on the radioactive aerosols. Powder mixtures have been chosen to have a quasi-homogeneous composition in the laser shot area because a complete simulation of a full-size source is not possible using our set-up, and the heating of such an inhomogeneous sample could introduce other variables in our studies, such as the preferential vaporization of one of the compounds. Different compositions of the mixed compounds have been created, as the variety of commercial radioactive source assemblies prevents from defining a unique source composition. Moreover, depending on the RDD design, and the explosion characteristics, the contribution to the vapour phase of cladding and source materials can vary, as reported in [6]. Thus, we have tested first pellets with an equal amount (in mass) of the materials, and subsequently also tested the influence of an excess of one of the compounds.

A summary of the samples tested is presented in **Table 2** and their characteristics in **Table 3**. Successive tests on the same material showed that the aerosol characteristics are reproducible under the same experimental parameters. Therefore, most experiments were performed once, due to the difficulty of working in a glove box and extensive time necessary for post-analyses.

For the cladding materials, tungsten has been chosen as it is one of the shields applied in nuclear medicine. Stainless steel is also applied in nuclear medicine as a second shield coupled with tungsten, or it is used as a unique cladding for metallic sources in sterilization plants or for radiography. The choice of the combination of cladding and source materials was made considering their application in the industry or in the medical facilities. For example, as Co and CsCl are used both in sterilization and in medical facilities, the cladding materials tested were both tungsten, stainless steel and a mixture of the two. Also testing of tungsten alone (without stainless steel) was performed, although this is not used in real applications, in order to understand the effect of this material on the aerosol characteristics. Finally for $SrTiO_3$, a radioactive source used for thermal generators, a wide range of cladding materials was applied in the past. These consist mainly of a first tungsten or lead shield, followed by a stainless steel container (as

Table 2. Samples tested in our studies, and the cladding materials investigated.

Sample	Cladding	Composition (%wt.)
Co	Tungsten	50/50, 30/70
	Stainless steel	50/50, 25/75
	Mixture	33/33/33, 22/71/7
CsCl	Tungsten	50/50, 25/75
	Stainless steel	50/50
	Mixture	33/33/33, 25/50/25
Ir	Stainless steel	50/50
$SrTiO_3$	Tungsten	50/50, 87.5/12.5
	Stainless steel	50/50
	Mixture	33/33/33, 25/50/25

Table 3. Properties of the applied materials in the experiments.

Sample	Purity	Grain size (μm)	*Vapour pressure (Pa) at 500 K	1000 K	2000 K	3000 K
Co	99.8	1.6	–	3.1×10^{-6}	2.1×10^{3}	9.5×10^{5}
CsCl	99.9		3.8×10^{-8}	97.3	1.24×10^{6}	–
Ir	99.9	<44	–	8.1×10^{-25}	3.3×10^{-5}	–
$SrTiO_3$	99	5	–	–	0.22 †	5.0×10^{4} †
W		$74 < X < 105$	–	–	2.4×10^{-10}	9.5×10^{-3}
				(1.4×10^{-7})	(2.8×10^{5})	
Steel	99.9	15	–	–	37.4	5.6×10^{4}

*Vapour pressure data were obtained from literature data [12] and described for the relevant temperature region for our experiments. The values in parentheses for W refer to WO_3.
†No data available. $SrTiO_3$ decomposes to SrO and TiO_2 during vaporization, as reported for $PbTiO_3$ in [13]. The vapour pressure values refer to SrO [12].

reported in [14,15]). In our experiments, tungsten and stainless steel were tested as cladding materials, to be consistent with the other tests.

3. Results

3.1. Co

Co is one of the materials applied in the feasibility study of the leaser heating approach, and the first results have already been presented by Di Lemma et al. [5]. Here some new results are presented that are important for the source term evaluation. The Co aerosols collected from our experiments show a classical bimodal size distribution (**Figure 1**). A first concentration maximum is found for particles with an AED > 10 μm; the other is found at around 400 nm. By fitting the first peak of the distribution with a log-normal curve, we obtain the mean mass diameter $\mu = 780$ nm and its standard deviation ($\sigma = 680$ nm). Applying the MOUDI impactor for the collection of the particles, the aerosol morphology as a function of the AED could be studied (as shown in **Figure 2**).

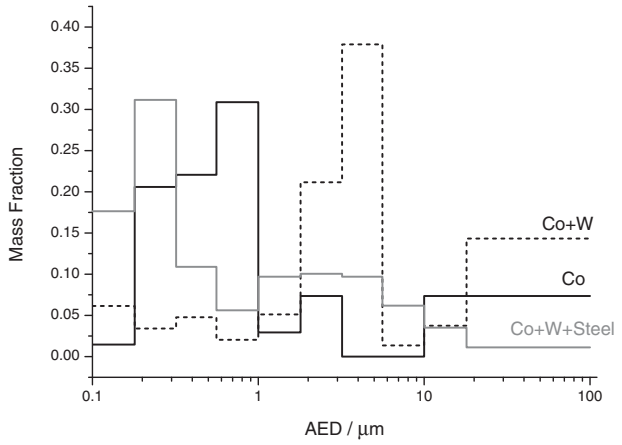

Figure 1. Aerosol size distribution for the Co sample and its mixture with the cladding materials, obtained by weighing the MOUDI impactor plates before and after the experiments.

It has been observed that spherical micrometre-size particles are mainly collected in the first stages (with a bigger AED cut-off size, which is seen as the first maximum of the size distribution), while the nanoparticle agglomerates are collected in the last stages with a smaller AED cut-off size (which corresponds to the peak in the nanometric range).

These different morphologies depend on the formation mechanism, as explained above. The micrometre-size particles are related to the dispersion of part of the liquid layer due to mechanical forces or shear forces generated by the thermal shock from the rapid laser energy transfer to the melted sample surface. The smaller nanometric particles are formed by a rapid quenching of the

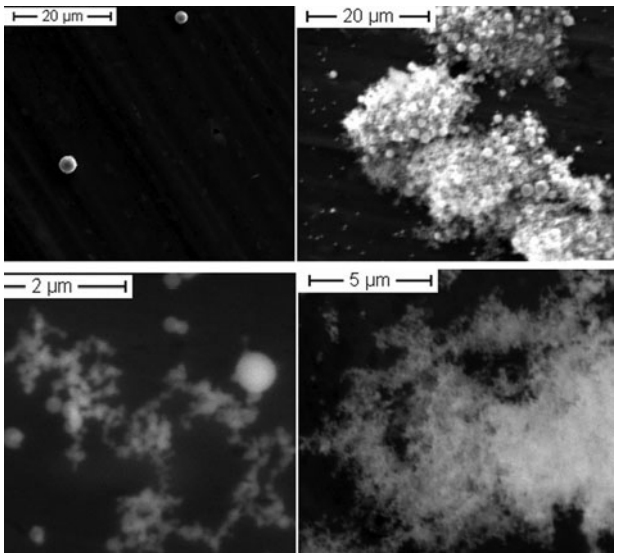

Figure 2. Examples of aerosols from the Co sample, showing the different types of particles: in the first stages (top left, with cut-off sizes 1.8 < AED < 18 μm), individual spherical particles were found; in stage 5 (top right, with a cut-off size of AED 1 μm), agglomerated particles were observed (a magnified image of these agglomerates is shown in the bottom-left frame). Nanometric agglomerates were found in the last stages 6–8 (bottom right, AED < 0.56 μm).

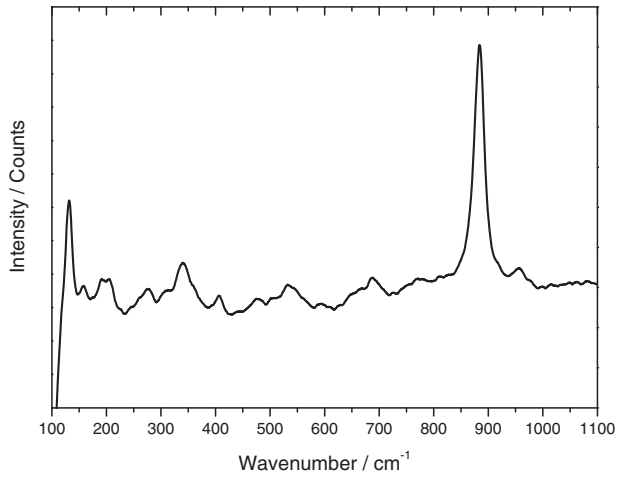

Figure 3. Raman spectrum measured for mixed cobalt–tungsten aerosols, showing all the typical bands of $CoWO_4$, as reported in [17–19].

vapour released in contact with the colder gaseous environment at room temperature. These particles will not coagulate to form bigger primary particles but will instead agglomerate in complicated structures (fractal-like structures) [16]. These agglomerates will then fold on themselves (as shown in Figure 2) due to the high number of primary particles.

3.2. *Co and the cladding*

Post-analyses of the mixed samples showed that the cladding materials did not influence the characteristic morphology of the aerosols. A shift of the peak in the nanometric size range to a bigger size was observed for the sample in the presence of tungsten (corresponding in the size distribution to a shift of $\mu = 4.3$ μm, with $\sigma = 480$ nm), as shown in Figure 1. This is related to the higher total mass of the aerosols released in this experiment. This higher quantity of vaporized material results in higher agglomeration rates, as a higher concentration of primary particles will be present in the system. As a result, more agglomerates will be generated, shifting the peak to a bigger AED ($\mu = 4.3$ μm). This higher total mass released in the presence of tungsten was caused by the higher vapour pressure of tungsten oxide in comparison to cobalt and its oxides (as shown in Table 3). Tungsten has a stronger tendency to oxidation compared to cobalt, as is evident from Ellingham diagrams, which causes the difference in their release.

The Raman spectroscopy analyses of the nanometric particles (0.18 < AED < 1 μm) also indicated a chemical interaction between tungsten and cobalt (as observed in **Figure 3**), resulting in the formation of $CoWO_4$ (our spectra were compared with the ones reported in [17–19]). The formation of $CoWO_4$ could also be inferred by the EDX analyses, which showed a Co/W ratio of 1 in these agglomerates. A change in the elemental composition was observed throughout the impactor stages in this test by SEM/EDX. Aerosols rich in tungsten were collected mostly in the stages with AED < 0.32 μm, as nanometric agglomerates. In these stages also, cobalt–tungsten mixed aerosols with a Co/W ratio ca. 1 were observed (as shown in **Figure 4**). It was not possible to observe tungsten oxides by Raman spectroscopy, indicating that the main compound vaporized could be $CoWO_4$ (209 w, 275 vw, 340 m, 408 w, 536 w, 686 m, 768 w, 881 s cm^{-1}) and not WO_3 (133 w, 268 m, 328 w, 712 m, 806 s cm^{-1}, as reported in [20]). Mixed Co/W aerosols were also observed in the stages with 0.56 < AED < 1.8 μm, while separated spherical particles and

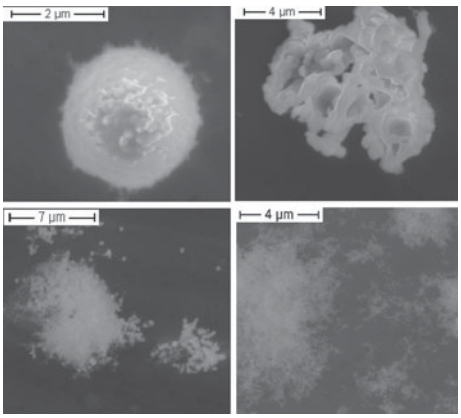

Stages	AED (μm)	Average Concentration (%wt.)	Maximum concentration (%wt.)	
0-4	1.8<AED <18	Co 78.5, W 21.5	Co 98.9, W 1.1	Co 8.0 W 92.0
5-8	0.18<AED <1.8	Co 20.9, W 79.1	Co 49.3, W 50.7	Co 7.4, W 92.6

Figure 4. Examples of aerosols from a mixed cobalt–tungsten sample (50/50%wt.), showing the different particles collected: top, aerosols collected from the first stages (1.8 < AED < 18 μm), isolated big particles and externally mixed agglomerates; bottom, mixed agglomerates containing Co and W, in the smaller particles, a higher content of tungsten was detected by SEM/EDX. The table shows the average concentration together with the maximum value detectable by EDX.

irregularly shaped aerosols of the individual starting materials, containing predominantly cobalt, were observed in the stages with bigger AED (1.8<AED<18 μm, as observed in Figure 4).

Also for tests conducted with cobalt and stainless steel, an elemental partitioning in the different size ranges was observed. Single spherical particles were observed in the stages with a cut-off size 3.2 < AED < 18 μm. In these stages, it was possible to observe isolated particles containing just Co or the cladding material (Fe, Cr). Agglomerates were found in the further stages with a progressively smaller primary particle diameter until nanometric agglomerates appeared in stage 6 (cut-off size: AED of 0.56 μm). These aerosols contained Fe and Cr, while cobalt was present as a minor component. Raman analyses showed for these stages only the presence of steel-related phases, such as magnetite, ferrite or chromite (comparing our spectra with the ones of Hanesch [21]). This indicates that stainless steel is the main material vaporized in these tests.

The mixture of cobalt, tungsten and stainless steel, intended to simulate a multiple cladding system, finally showed a peculiar behaviour. Low concentrations of tungsten were detected by EDX at all impactor stages (<4%$_a$), and by Raman spectroscopy it was not possible to detect chemical compounds containing tungsten. The bands in the Raman spectrum were solely related to phases formed from steel (such as magnetite, ferrite or chromite [21]). This mixture had a behaviour as if only stainless steel was present. This could indicate that tungsten is not vaporized in these tests but retained in the pellet. To check for this possibility, analyses of the pellet by EDX were performed after the test. These analyses showed a higher concentration of tungsten in the laser shot area with respect to the unmelted material. All of this indicates that tungsten is retained in the pellet, possibly by the formation of a stable alloy with iron and chromium. This alloy could prevent tungsten vaporization. Consequently, cobalt, the source material, behaved similarly to the case in which only stainless steel was present as cladding material, and was found as isolated particles in the first stages. Finally, in these tests the size distribution shows only a peak in the smaller nanometric size range (Figure 1, $\mu = 256$ nm $\sigma = 504$ nm), which can be explained by the fact that a high melting point material (stainless steel) was vaporized as the major compound, which was quenched quickly to solid particles with a small diameter.

The following is a summary of the results for the cladding–source interaction:

- Tungsten had a strong effect on the release, changing the size distribution and creating a new compound.
- Stainless steel did not interact with the simulated source material and was the main material observed in the aerosols.

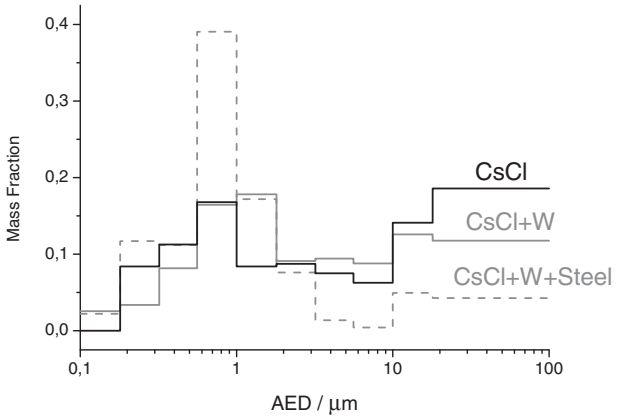

Figure 5. Aerosol size distribution for the CsCl sample and its mixture with the cladding materials, obtained by weighing the MOUDI impactor plates before and after the experiments. The size distribution refers to a CsCl + W + Steel mixture (25/50/25 composition), with may explain the minimal shift of the peak to $\mu = 1.11$ μm ($\sigma = 600$ nm).

- Finally, when the mixture of tungsten and stainless steel as cladding materials was tested, the sample behaved as if only stainless steel was present. Tungsten was observed to be retained in the pellet, not participating in the aerosol formation process.

3.3. *CsCl*

The aerosol characterization from this material was presented in [5]. This material revealed the highest total aerosol mass released among the source materials tested in this study. This is related to the higher vapour pressure of this compound with respect to the other sources tested (as shown in Table 3). The size distribution of the collected aerosols showed a bimodal shape (as shown in Figure 5), the peak in the nanometric size range corresponding to a log-normal size distribution, with $\mu = 873$ nm and $\sigma = 511$ nm.

Analysis by Raman spectroscopy was not possible as first-order vibrations are not allowed due to the crystal symmetry of CsCl. Additional tests with different levels of humidity were also performed (ca. 20%, 50%, 90% relative humidity at room temperature) and for these Raman analyses were carried out to verify the presence of hydrates or hydroxide. These should show a broad peak between 3000 and 3700 cm^{-1}. However, this peak could not be detected, indicating that CsOH was not formed in these tests. This could be due to the low saturation value of water in air at room temperature.

3.4. *CsCl and the cladding*

The influence of cladding on the aerosol characteristics has been studied, testing tungsten and a mixture of tungsten and stainless steel also for the CsCl sample. The cladding material did not influence the characteristic morphology of the aerosols, but a higher mass release was detected in the presence of tungsten, similar

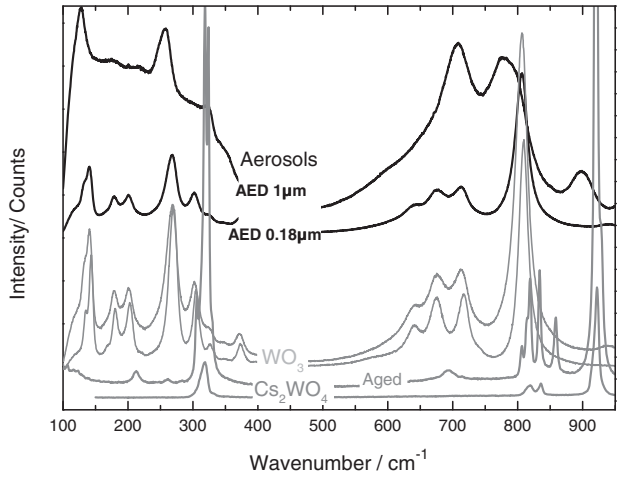

Figure 6. Results from the Raman analyses on the aerosols produced from a mixture of CsCl and W, showing a chemical partitioning over the different stages. Smaller particles show the presence of WO_3. The middle stages show some modification in the spectra (e.g. 320, 700–780 and 900 cm^{-1} bands) that are related to the formation of a new chemical compound.

to the cobalt experiments. This higher mass release is related to the higher temperature reached in the presence of tungsten, because it adsorbs better the laser light with respect to CsCl (as it has an higher emissivity), and it acts as a thermal conductor. Also in this experiment the higher release leads to a shift of the peak in the accumulation mode (nanometric size range) to a bigger AED (as shown in Figure 5, to $\mu = 1.6$ µm, $\sigma = 600$ nm), which can be explained by the faster agglomeration rates, due to the higher concentration of primary particles.

An influence of the tungsten cladding material was observed also for the elemental partitioning studied throughout the impactor stages:

- The first stages ($3.2 < \text{AED} < 18$ µm) showed isolated aerosols containing either CsCl or W.
- In the middle stages ($0.56 < \text{AED} < 3.2$ µm), mixed agglomerates containing both compounds were found.
- While in the last stages ($0.18 < \text{AED} < 0.56$ µm), aerosols with a high concentration of W were observed.

Also a clear difference in the Raman spectra could be observed between the different stages, confirming a chemical partitioning: the stages 7–8 ($0.18 < \text{AED} < 0.56$ µm) contained principally WO_3, whereas the AED stages with a cut off size $0.56 < \text{AED} < 1$ µm revealed complex and different spectra (as shown in **Figure 6** for the stages 5 and 8, with a cut-off AED between 1 and 0.18 µm). New bands at 320, 700–780 and 900 cm^{-1} were detected. For the stages with a cut-off size $1 < \text{AED} < 0.56$ µm (as shown in Figure 6 for stage 5), the comparison of the Raman spectra appeared difficult. The aerosols collected revealed intense absorptions (133 w, 268 m, 328 w, 712 m, 806 s cm^{-1}) corresponding to WO_3 (using literature data by Haro-Poniatowski et al. [22]), indicating a high concentration of this compound. A minor contribution from another phase (low-intensity bands) was observed, and this phase was attributed to Cs_2WO_4 aged in air. Because the Raman spectrum of Cs_2WO_4 was not reported in literature, we measured the reference spectra of the pure compound (obtained from INTERFINE CHEMICALS) as well as the compound aged in air (hydrated under the atmospheric environmental conditions) in this work.

The mixture of CsCl with tungsten and stainless steel showed a similar behaviour to that observed for the case of cobalt, i.e. tungsten was not detected in the aerosols. Increasing the tungsten content (from 33%wt. to 50%wt. as shown in Table 2) in the sample did not significantly increase the tungsten concentration detected by SEM/EDX in the aerosols, indicating that tungsten was always the minor compound vaporized. Stainless steel related phases were instead observed by EDX in all size ranges, while Cs and Cl were observed mainly in the first stages ($3.2 < \text{AED} < 18$ µm), and attached to bigger particles of stainless steel. On the other hand, the vaporized stainless steel seems not to interact chemically with CsCl. Variation of the chemical composition of the aerosols was not detected by Raman spectroscopy, and the only species observed were stainless steel related phases. However, when the tungsten content in the sample was high, it was possible to observe some Raman bands that could not be assigned to stainless steel phases and showed characteristics of the Cs_2WO_4 spectrum. From this we can conclude that tungsten is mainly retained in the pellet in the presence of stainless steel, and by increasing the tungsten concentration, it is possible to force the vaporization of a small amount of tungsten, mainly in the form of a new chemical compound (possibly Cs_2WO_4).

The following is a summary of the results for the cladding–source interaction for CsCl samples:

- Again tungsten seems to have an high effect on the release, leading to a higher total aerosol mass collected, changing the size distribution and creating a new compound.
- When the mixture of cladding materials was tested, the sample behaved as if just stainless steel was present. When an excess of tungsten was present in the sample, it was possible to detect a new phase in the aerosols (possibly Cs_2WO_4).

3.5. *Ir*

The Ir sample showed a strong resistance to oxidation. The vapour pressure of this material, both in the metal form and in the oxide form, is lower than for all the other tested compounds (as shown in Table 3). This resulted in the lowest quantity (total mass) of aerosols

collected. The aerosols revealed a similar morphology to the other test materials: micrometre-size spherical particles and nanometric agglomerates in fractal-like structures. The size distribution was difficult to measure due to the low mass collected which resulted in high uncertainties due to the detection limit of the balance.

Analysis of these particles by SEM/EDX showed a low content of oxygen in all the particles. Raman spectroscopy of the collected particles also did not reveal the characteristic bands of IrO_2, and showed a high fluorescence. All of this may suggest that the sample is vaporized as metallic Ir, and in fact this fluorescence behaviour has been reported for the Ir metal [23]. On the other hand, when the pellet was analysed by Raman spectroscopy, the bands of IrO_2 could be detected on the laser melted area (as reported in [24]). The discrepancy between aerosols and the oxidation state of the pellet can be explained by the fact that the oxidation occurs during the cooling of the pellet when aerosols are no longer released. Moreover, iridium oxides are reported to decompose to the metal [25] in the temperature range of our experiments.

3.6. *Ir and the cladding*

For this sample, only stainless steel was tested, as this is the main cladding applied with iridium. The aerosols did not show major morphology differences. The main material vaporized was again stainless steel, which was found as a mixture of magnetite, ferrite and chromite throughout all the stages. Ir was detected just in the first stages ($3.2 < \text{AED} < 18$ μm), and was collected as big spherical isolated particles or as externally mixed aerosols with Fe and Cr.

The possibility of a chemical interaction between these materials had been excluded by Raman analyses, which showed only the bands of the oxidized steel phases. It can be concluded that there was no high release for Ir in our experiments, and also it did not interact chemically with the cladding material tested. This results in the low total mass released.

3.7. *$SrTiO_3$*

For $SrTiO_3$ a similar morphology and size distribution of the aerosols were found compared to other materials tested (**Figure 7**, $\mu = 470$ μm), showing big micrometre-size spherical particles and agglomerates of smaller nanometric aerosols. Moreover, at the pre-stage (AED > 18 μm) also, solid fragments were observed, related to the ejection of pieces of the unmelted material from the pellet. This phenomenon may be caused by the high stress in the brittle pellet, caused by the thermal shock imposed by the laser pulse.

EDX analyses of the aerosols showed no sign of dissociation of the initial compound, the particles containing always Sr and Ti in equal amount. Finally, Raman spectroscopy permitted to observe differences between the pellet and the collected aerosols (as shown in **Figure 8**): the former showed the typical broad bands of the $SrTiO_3$ crystal (as reported in [26] at ca. 200–500 and 600–750 cm^{-1}), while the latter showed bands related to first-order vibrations (broad bands at ca. 550 and 800 cm^{-1}). As explained in literature [27,28], defects, size effects or strains can break the symmetry of the crystal and allow the detection of first-order Raman bands. Moreover, for the particles with a cut-off size AED of 1 μm, the spectrum was similar to that of the $SrTiO_3$ crystal. This shows that this effect is less visible for particles with a bigger dimension and is related to the nanometric dimension of the particles in the lower stages of the MOUDI impactor.

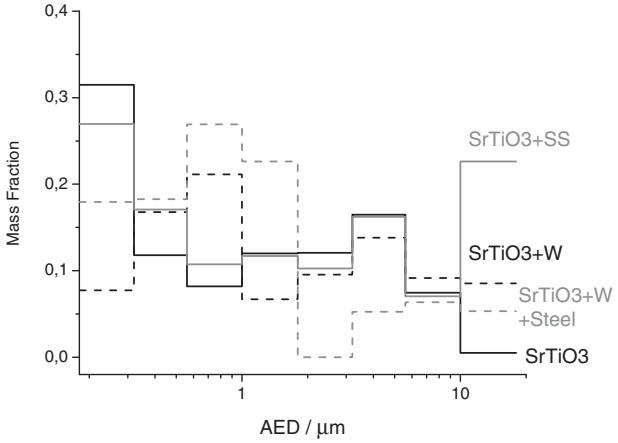

Figure 7. Aerosol size distribution for the $SrTiO_3$ sample and its mixture with the cladding materials, obtained by weighing the MOUDI impactor plates before and after the experiments.

3.8. *$SrTiO_3$ and the cladding*

The experiments with cladding materials showed similar results to those in the experiments performed

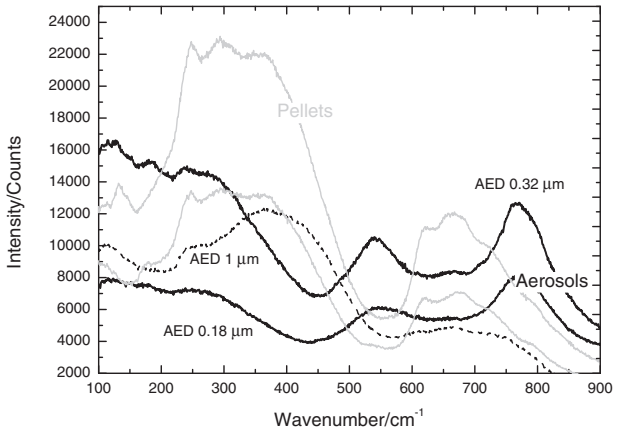

Figure 8. Raman spectra for the $SrTiO_3$ aerosols and pellets, showing the difference between the bulk material and the first-order bands related to the nanometric aerosols. In particular, the spectrum of the particles in the stage 5 (AED of 1 μm) is similar to the bulk material, indicating that this effect becomes evident only for smaller particles.

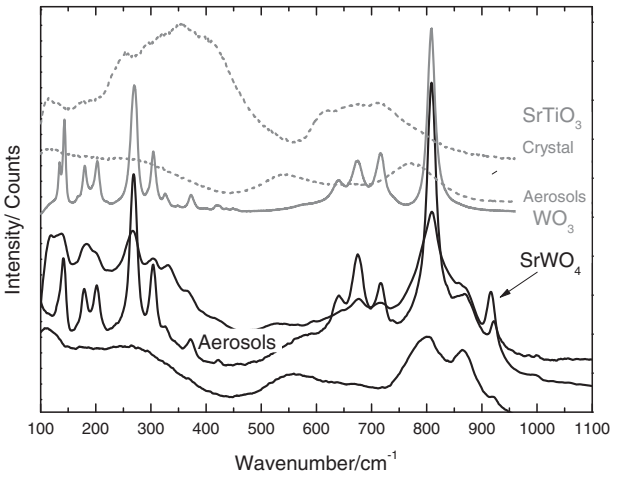

Figure 9. Typical Raman spectra for the aerosols collected from an $SrTiO_3$ sample with tungsten, showing a chemical partitioning with AED. In the smaller particles, the bands of WO_3 can be observed. The formation of $SrWO_4$ can be inferred from the band at 922 cm^{-1}.

for the other sources. The morphology of the particles was not influenced by the presence of the cladding material, while the chemical composition of the aerosols showed modifications. For this experiment, the total aerosol mass released was not influenced by the cladding material and the total mass released was similar for all the experiments. Finally, a shift of the peak in the nanometric size range was observed in the presence of tungsten (Figure 7, $\mu = 750$ μm) but not when stainless steel was tested.

When tungsten was included in the sample, the formation of a new compound was detected by Raman spectroscopy (shown in **Figure 9**, from the band at 922 cm^{-1} as compared with the data for $SrWO_4$ by Zhao et al. [29]). Moreover, an elemental partitioning was observed in the presence of tungsten:

- Nanometric particles, collected in the lower stages ($0.18 < AED < 0.56$ μm), were enriched in the cladding material. These showed the bands of WO_3 by Raman spectroscopy.
- In the intermediate stages ($0.56 < AED < 1$ μm), mixed aerosols were found. These aerosols showed by Raman analyses the bands related to a new compound.
- Finally, in the bigger particle ($AED > 1$ μm), isolated initial compounds were detected by EDX, the particles containing either the source material or the cladding material.

On the other hand, when stainless steel was included in the sample, no chemical interaction with the source material was observed. In this case, phases related to the cladding material (stainless steel) were collected as the main components of the aerosols throughout all the stages. The Raman spectra showed just the bands of the stainless steel related phases in all the stages. In the prestage of the impactor, aerosols containing the initial isolated compounds were detected.

Finally, when stainless steel and tungsten were present together as cladding materials, a low content of tungsten was detected in the collected aerosols. The aerosols showed similar features to those for the stainless steel cladding test.

The results for $SrTiO_3$ can be summarized as follows:

- Tungsten showed a chemical interaction with the source material, and in that case a chemical partitioning with the AED was observed.
- Stainless steel, on the other hand, did not interact with the simulated source material and stainless steel related phases were the main materials detectable in the aerosols.
- Tungsten was retained and not vaporized when the mixture of cladding materials was tested. The sample behaved as if only stainless steel was present.

4. Discussion and conclusions

It should be emphasized that the mass and size distribution of the air-borne material are the main parameters for the evaluation of the effects of an RDD explosion. Integral experiments [6,8] using explosives showed that the particles released from such events could be divided into big micrometre-size particles (related to the mechanical impact of the explosion) and smaller nanometric particles (related to the vaporization process resulting from the high temperature created). The smaller particles are generally the most dangerous as they are air-borne and inhalable and can be transported over larger distances. Aerosol release related to the vaporization of the sample is consequently the main feature to be investigated for risk assessment.

In our experiments, these particles were produced by vaporization of the sample using a laser heating technique, which permits to obtain rapid high temperature transients and mimic the RDD temperature conditions. The particles are formed by a rapid quench of the vapour released from the sample in a cooler air environment. Thus, it is possible to study the vaporization process and the influence of interaction with other materials on the aerosol characteristics. However, it is also clear that the conditions of a real detonation cannot be simulated by the system, due to the difficulty in reproducing an explosive wave in the set-up.

We have observed a bimodal size distribution in our experiments, similar to that reported in literature for integral experiments [6,8]. Micrometre-size particles were collected together with nanometric particles in our experiments, related to the ejection of material by the mechanical shock of the laser shot. This can be liquid material from the laser melted area which creates spherical micrometre-size particles, or solid irregular-shaped fragments generated from the unmelted pellet. It was

possible with our tests to investigate the different characteristics of the particles in these two size ranges, although the fractional release between the two types of aerosols cannot reproduce that of an RDD detonation.

Different release characteristics were observed for the different sources studied:

- CsCl showed the highest total mass released. The aerosols collected had the same chemical composition as the initial sources.
- Co aerosols were collected in lower mass with respect to CsCl, and the particles were mainly composed of cobalt oxides.
- Ir revealed the lowest vaporization, due to low vapour pressure and high oxidation resistance. Particles were collected in the metallic form.
- $SrTiO_3$ showed a similar morphology and mass release to that of cobalt, but the aerosols collected kept their initial composition.

Our test focused also on the effect of the source–cladding interaction on the aerosol release. The results can be summarized as follows:

- CsCl particles were collected only in bigger AED in the presence of stainless steel. In the presence of tungsten, a different chemical partitioning with AED was observed. The bigger particles were isolated aerosols containing CsCl or WO_3. In the middle stages, mainly mixed compound aerosols were found, and the formation of Cs_2WO_4 was observed. Finally, in the smaller AED, the main aerosol species were related to W compounds. The total mass released was higher in the presence of tungsten.
- Co was found in low quantity in the aerosols in the presence of stainless steel. In the presence of tungsten, cobalt forms $CoWO_4$ aerosols. These were collected at all the stages of the impactor, also in the one with the smallest AED.
- Ir was found just with AED > 3.2 μm when in the presence of the cladding material.
- $SrTiO_3$ showed a chemical reaction when W was used as a cladding material with the formation of a new compound. No interaction with stainless steel was observed.

From these results, it can be concluded that the presence of stainless steel does not lead to a chemical interaction with the tested source materials. The aerosols containing the simulated radioactive materials are concentrated in the higher AED, leading to a lower probability of inhalation in the lungs. Tungsten instead seems to have a substantial effect, as an increase of the total mass release was observed. This can be related to the creation of more volatile compounds but can also be caused by a heat transfer mechanism typical for our set-up. Although in this case a shift to bigger AED was observed, it was minimal, not affecting the risk by inhalation in the lungs (AED < 10 μm). In all cases (except iridium), tungsten showed a chemical interaction with the source materials, creating new chemical compounds (tungstates). This chemical interaction has a strong effect on the aerosol formation process as a compound with a different thermo-physical property is created. This could result in a change of the coagulation and collision rates, which could concentrate the radioactive source material in a particular size range. Consequently, it must be considered in the evaluation of the radiological consequences of an RDD explosion.

When the two cladding materials were tested together, retention of tungsten was observed in the sample by the formation of an alloy with iron and chromium. This prevented its interaction with the source material in the gaseous phase, and the samples tested behaved as if only stainless steel was present. This effect is probably typical for our experiments in which the source material and the cladding materials were mixed as powders, thus easing the alloy formation and preventing vaporization of tungsten. It must be investigated if this reaction could occur in a real RDD explosion.

Finally, we can compare our findings to the observations of the integral tests. In the tests of Harper et al. [6], no chemical reactions were observed, and the soil entrained in the fireball was observed to interact with the radioactive materials only by agglomeration and/or coagulation, affecting the size of the "radioactive" particles. However, we should point out that minor chemical analyses were performed on the particles, which did not exclude chemical interactions. On the other hand, in the tests of Lee et al. [8] on CsCl, the effect of chemical interaction on the source was clearly observed (such as a different ratio of Cs to Cl in the aerosols), without identifying its cause. Our work clearly shows the importance of detailed characterization of the aerosols and the usefulness of separate effect studies to effectively investigate the mechanisms of aerosol formation from the vapour phase, the chemical reactions and their influence on the aerosol characteristics.

We can conclude that with our tests we were able to study the vaporization–condensation process occurring in dirty bombs detonations in controlled laboratory conditions. In particular, we could produce and investigate the nanometric particles of greatest interest for the risk assessment of RDD explosions. An important outcome of our work is the observation of the possibility of an elemental and chemical partitioning with AED of the particles produced when interaction with the cladding material of the source occurs. This can influence the assessment of the extension and level of the contaminated area using radioactive dispersion codes which need to be included in the description of the source term for such calculations. Our tests thus emphasize the importance of studying not only the cladding materials of the source, but also other materials of interest that

could chemically or physically interact with the source material.

Acknowledgements

This work was supported by the 7th Framework Program of the European Commission.

Disclosure statement

No potential conflict of interest was reported by the authors.

References

[1] Medalia J. Dirty bombs: technical background, attack prevention and response, issues for congress (Report n. R41890). Congressional Research Service (US); 2011.
[2] Shin H, Kim J. Development of realistic RDD scenarios and their radiological consequence analyses. Appl Radiat Isot. 2009;67(7–8):1516–1520.
[3] Magill J, Hamilton D, Lützenkirchen K, et al. Consequences of a radiological dispersal event with nuclear and radioactive sources. Sci Global Security. 2007;15(2):107–132.
[4] Andersson KG, Mikkelsen T, Astrup P, et al. Requirements for estimation of doses from contaminants dispersed by a dirty bomb explosion in an urban area. J Environ Radioact. 2009;100(2):1005–1011.
[5] Di Lemma FG, Colle JY, Ernstberger M, et al. RADES an experimental set-up for the characterization of aerosol release from nuclear and radioactive materials. J Aerosol Sci. 2014;70(5):36–49.
[6] Harper FT, Musolino SV, Wente, WB. Realistic radiological dispersal device hazard boundaries and ramifications for early consequence management decisions. Health Phys. 2007;93(1):1–16.
[7] Prouza Z, Beckova V, Cespirova I, et al. Field test using radioactive matter. Radiat Prot Dosim. 2010;139(4):519–531.
[8] Lee SD, Snyder EG, Willis R, et al. Radiological dispersal device outdoor simulation test: cesium chloride particle characteristics. J Hazard Mater. 2010;176(1–3):56–63.
[9] Simpson R, Fried L, Ree F, et al. Unraveling the mystery of detonation. Sci Tech Rev. 1999 June:12–18.
[10] Reinhart WD, Thornhill TF, Chhabildas LC, et al. Temperature measurements of expansion products from shock compressed materials using high-speed spectroscopy. Int J Impact Eng. 2008;35:1745–1755.
[11] Andersson KG, Mikkelsen T, Astrup P, et al. Estimation of health hazards resulting from a radiological terrorist attack in a city. Radiat Prot Dosim. 2008;131(3):297–307.
[12] Yaws CL, Prasad NR, Chaitanya G. The Yaws handbook of vapor pressure: antoine coefficients. Houston (TX): Gulf Publishing Company; 2007.
[13] Kobertz D, Mueller M, Molak A. Vaporization and caloric studies on lead titanate. Calphad. 2014;46:62–79.
[14] Standring WJF, Dowdall M, Sneve M, et al. Assessment of environmental, health and safety consequences of decommissioning radioisotope thermal generators (RTGs) in Northwest Russia (Stralevern Rapport 2005:4). Osteras: Statens stralevern, Norwegian Radiation Authority; 2005. Available from: http://www.nrpa.no/dav/c600d1d288.pdf
[15] Heard R. IAEA action to improve the management of disused sealed radioactive sources (DSRS) including RTGs. Paper presented at: CEG; 2008 April 23–24; Vienna.
[16] Friedlander SK. Smoke, dust, and haze: fundamentals of aerosol dynamics. 2nd ed. Oxford: Oxford University Press; 2000.
[17] Thongtem S, Wannapop S, Thongtem T. Characterization of $CoWO_4$ nano-particles produced using the spray pyrolysis. Ceram Int. 2009;35(5):2087–2091.
[18] Sujana-Kumari U, Suresh P, Prasada-Rao AV. Grinding-assisted solid-state metathetic synthesis of divalent transition metal tungstates. Pure Appl Chem. 2013;3(1):1–9.
[19] Ruiz-Fuertes J, Errandonea D, López-Moreno S, et al. High-pressure Raman spectroscopy and lattice-dynamics calculations on scintillating MgWO: comparison with isomorphic compounds. Phys Rev B: Condens Matter. 2011;83(21):214112–214123.
[20] Wu W, Yu Q, Lian J, et al. Tetragonal tungsten oxide nanobelts synthesized by chemical vapor deposition. J Cryst Growth. 2010;312:3147–3150.
[21] Hanesch M. Raman spectroscopy of iron oxides and (oxy)hydroxides at low laser power and possible applications in environmental magnetic studies. Geophys J Int. 2009;177:941–948.
[22] Haro-Poniatowski E, Jouanne M, Morhange JF, et al. Micro-Raman characterization of WO_3 and MoO_3 thin films obtained by pulsed laser irradiation. Appl Surf Sci. 1998;127–129:674–678.
[23] Downs RTM. The RRUFF Project: an integrated study of the chemistry, crystallography, Raman and infrared spectroscopy of minerals. Paper presented at: 19th General Meeting of the International Mineralogical Association 2006; 2006 July 23–28; Kobe.
[24] Korotcov AV, Huang YS, Tiong KK, et al. Raman scattering characterization of well-aligned RuO_2 and IrO_2 crystals. J Raman Spectrosc. 2007;38:737–749.
[25] Sanjinds R, Aruchamy A, Lévy F. Thermal stability of sputtered iridium oxide films. J Electrochem Soc. 1989;136(6):1740–1743.
[26] Merkulov VI, Fox JR, Li HC, et al. Metaloxide bilayer Raman scattering in $SrTiO_3$ thin films. Appl Phys Lett. 1998;72(25):3291–3293.
[27] Du YL, Chen G, Zhang MS. Investigation of structural phase transition in polycrystalline $SrTiO_3$ thin films by Raman spectroscopy. Solid State Commun. 2004;130:577–580.
[28] Rabuffetti FA, Kim HS, Enterkin JA, et al. Synthesis-dependent first-order Raman scattering in $SrTiO_3$ nanocubes at room temperature. Chem Mater. 2008;20:5628–5635.
[29] Zhao X, Cheung TLY, Zhang X, et al. Facile preparation of strontium tungstate and tungsten trioxide hollow spheres. J Am Ceram Soc. 2006;89(9):2960–2963.